Published in final edited form as:
Nat Microbiol. 2019 June ; 4(6): 1006–1013. doi:10.1038/s41564-019-0379-8.

Social evolution of innate immunity evasion in a virus

Pilar Domingo-Calap, **Ernesto Segredo-Otero**, **María Durán-Moreno**, and **Rafael Sanjuán***
Institute for Integrative Systems Biology (I2SysBio), Universitat de València - Consejo Superior de Investigaciones Científicas, C/ Catedrático Agustín Escardino 9, 46980 Paterna, València, Spain

Abstract

Antiviral immunity has been studied extensively from the perspective of virus-cell interactions, yet the role of virus-virus interactions remains poorly addressed. Here we demonstrate that viral escape from interferon (IFN)-based innate immunity is a social process in which IFN-stimulating viruses determine the fitness of neighbor viruses. We propose a general and simple social-evolution framework to analyze how natural selection acts on IFN shutdown, and validate it in cell cultures and mice infected with vesicular stomatitis virus (VSV). Additionally, we find that IFN shutdown is costly because it reduces short-term viral progeny production, thus fulfilling the definition of an altruistic trait. Hence, in well-mixed populations the IFN-blocking wild-type virus is susceptible to invasion by IFN-stimulating variants, and spatial structure consequently determines whether IFN shutdown can evolve. Our findings reveal that fundamental social evolution rules govern viral innate immunity evasion and virulence, and suggest possible antiviral interventions.

Social interactions have shaped the evolution of organisms from bacteria to animals. Social evolution has been investigated using various approaches including kin selection, group selection, and game theory1–3, but has been seldom validated empirically in viruses4. A major limitation has been our lack of mechanistic understanding of how social interactions take place in viruses. For instance, a landmark study showed that experimental populations of bacteriophages obey Prisoner´s dilemma5, but the underlying mechanisms were not elucidated. More recently, it was suggested that hepatitis C virus undergoes so-called “antigenic cooperation”, whereby virus variants eliciting broad cross-reactive antibodies facilitate the persistence of other variants6. However, the details of such interactions were not clarified.

Some molecular processes potentially allowing for social interactions among viruses have been characterized. For instance, certain phages secrete a short peptide that signals viral

*Correspondence and requests for materials should be addressed to rafael.sanjuan@uv.es.

Data availability. No restrictions apply to data availability. Relevant data are provided in the manuscript and the Supplementary Information. All data are available from the corresponding author upon request. No new protein, DNA or RNA sequence data, macromolecular structures, crystallographic data or microarray data requiring deposition in public repositories were produced.

Author information. The authors declare no conflict of interest.

Author contributions. P.D-C. performed the cell culture experiments. E.S-O. contributed to designing the model. M.D-M. performed the animal experiments. R.S. conceived the study, formulated the model, analyzed the data, and wrote the manuscript.

Europe PMC Funders Author Manuscripts

population density and guides lysis-lysogeny decisions7. Also, some phage-encoded proteins partially antagonize but not fully suppress anti-phage CRISPRs, which might allow for cooperation if co- or super-infecting phages sum up the effects of their proteins8. Potentially cooperative interactions have also been reported between neuraminidase variants of influenza virus9. However, the social evolution of these virus-virus interactions has not been explored. More generally, bottom-up approaches that link specific molecular mechanisms to population-level processes are needed to achieve a better understanding of social evolution not just in viruses, but also in different types of organisms10,11.

Innate immunity is the first line of defense against viruses and is triggered by recognition of pathogen-associated molecular patterns, leading to secretion of type-I interferons (IFNs) and other pro-inflammatory cytokines12,13. IFNs function in an autocrine manner by self-inducing antiviral responses in the infected cell, but also in a paracrine manner by signaling the infection locally and inducing a virus-resistant state in neighbor cells. In response, viruses have evolved various mechanisms to suppress IFN-mediated innate immunity13–15. We propose that the ability of a given virus to suppress IFN-mediated innate immunity modifies the fitness of other members of the viral population and, thus, is a social trait. Specifically, we predict that variants failing to prevent IFN secretion spark antiviral responses that inhibit the spread of neighbor viruses. We first model this process using a partition of viral fitness according to social neighborhood. This shows that the condition for IFN shutdown to evolve is analogous to the classical Hamilton rule3. We then demonstrate the social nature of IFN evasion in cell cultures and mice using IFN-stimulating and IFN-blocking VSV variants.

Theory

We consider two virus variants, one that blocks IFN secretion (W) and another that does not (D), and partition the fitness of each variant according to social neighborhood. Specifically, we call $f_{W/W}$ and $f_{W/D}$ the log-fitness of the W variant in a W neighborhood and a D neighborhood, respectively. Analogously, D fitness is partitioned into $f_{D/D}$ and $f_{D/W}$. For both variants, being in a W neighborhood has a positive effect b relative to being in a D neighborhood because IFN is not released from neighbor cells. Hence, b is determined by paracrine IFN action and measures indirect fitness effects. On the other hand, c is the direct effect on the actor virus of blocking IFN, independent of neighborhood. Blocking IFN secretion may provide a direct benefit through autocrine effects ($c < 0$), but may also entail costs ($c > 0$). We set the W virus in a W background as reference, such that $f_{W/W} = 0$. By definition, then, $f_{W/D} = -b$, $f_{D/W} = c$, and $f_{D/D} = c - b$ (Fig. 1). We define W fitness across neighborhoods as $f_W = r_W f_{W/W} + (1 - r_W) f_{W/D}$, where r_W is a parameter indicating how strongly W is influenced by neighbor viruses of its own type ($0 \leq r_W \leq 1$). Analogously, $f_D = r_D f_{D/D} + (1 - r_D) f_{D/W}$. Hence, $f_W = -b(1 - r_W)$ and $f_D = r_D(c - b) + c(1 - r_D) = c - r_D b$. Whether IFN suppression is favored by selection depends on the quantity $f_W - f_D$, which equals $(r_W + r_D - 1)b - c$.

We thus model IFN shutdown as a potentially costly, cooperative trait, which is favored by selection only if $(r_W + r_D - 1)b - c > 0$. By denoting $r = r_W + r_D - 1$ we recover Hamilton´s rule, $rb - c > 0$, a central result of kin selection theory3. Hence, r may be interpreted as a

measure of genetic relatedness. However, here r is more precisely defined as the difference between the social neighborhoods of W and D and describes spatial structure in terms of the immune response each variant receives. This spatial structure can vary from a loose assortment determined by IFN and viral diffusion to well-defined, isolated subpopulations. The effect of spatial structure on social evolution could also be modelled from a group selection perspective16,17, which is generally accepted to be formally equivalent to kin selection16–19. A particularity of this system is that the social process is mediated by a diffusible antiviral protein. Therefore, IFN acts in a manner opposed to classical public goods such as secreted enzymes20–22. Suppressing IFN secretion creates a space favorable to viral growth, analogous to preventing the release of a pollutant. However, the presence of IFN-stimulating neighbors could render cooperation ineffective. Based on this, we expect the D variant to exert a strongly negative effect on W, whereas the W variant may provide little benefit to D. In terms of the model, this prediction is stated as $r_D > r_W$. Finally, we note that demography is not explicitly implemented in the model and that, consequently, changes in the size and structure of the viral population or the immune response may result in time-dependent parameters.

Interaction between wild-type and IFN-inducer VSV variants

To test the social nature of IFN shutdown empirically we used VSV, a prototypic negative-strand RNA animal virus. The VSV matrix protein M suppresses host gene expression, preventing IFN production23. Mutations in M methionine 51 inactivate this function and attenuate VSV in IFN-competent cells24,25. Here, we used a deletion mutant (Δ51) carrying a GFP reporter and an isogenic wild-type virus (WT) carrying an mCherry reporter. Confirming previous work, we found by ELISA that mouse embryonic fibroblasts (MEFs) inoculated with the Δ51 virus at a multiplicity of infection (MOI) of 3 foci forming units (FFU) per cell secreted IFN-β extensively (1797 ± 108 units at 16 hours post inoculation, hpi; error terms indicate the standard error of the mean), whereas IFN remained undetectable in WT-infected cells. Similarly, mRNA levels of the IFN-stimulated anti-VSV effector Mx2 were 114.3 ± 8.1 times higher in MEFs infected with Δ51 than in those infected with WT.

Pure WT infections reached a final titer of 10^8 FFU/mL independent of the MOI at inoculation, whereas pure Δ51 infections reached a titer 10 to 200 times lower depending on the MOI (Fig. 2a). In MEFs infected with both variants the total viral yield decreased exponentially with the fraction of Δ51 at inoculation (Fig. 2b), indicating that WT fitness was adversely affected by Δ51. To show the involvement of cytokines in this interaction, we filtered the supernatant from a Δ51 infection to remove virions and collect small proteins including IFNs. Pretreatment of cells with this conditioned medium inhibited WT growth strongly and in a dose-dependent manner (Fig. 2c). This effect became weaker if the virus and the conditioned medium were added simultaneously, and was nearly lost if the conditioned medium was added >3 hpi (Fig. 2d). Hence, the ability of IFN to suppress virus production in already infected cells was limited, indicating that the role of IFN consisted mainly in protecting uninfected cells.

Spatial structure of infection and immunity

We first measured the area of influence of individual Δ51-infected cells. For this, we inoculated MEFs with Δ51-GFP at low MOI (<0.001 FFU/cell) and added a neutralizing monoclonal antibody (NmAb) following virus adsorption to prevent secondary infections. At 20 hpi, we added NmAb-resistant WT-mCherry virus (10 FFU/cell). This WT infected the entire culture except areas around Δ51-infected cells, which remained free of either virus (Fig. 2e). Therefore, Δ51 produced a spatially structured, negative influence on infection. We next used real-time fluorescence microscopy to investigate the spatial structure and dynamics of viral spread. To accomplish this, we performed pure and mixed (1:1 input) infections using WT and/or Δ51 variants (ca. 0.01 FFU/cell). Both viruses completed the first infection cycle and reached neighbor cells but, whereas pure WT infections progressed further until invading the entire culture, Δ51 infections were halted at around 20 hpi (Fig.3; Supplementary Fig. 1; Supplementary Video 1; Supplementary Video 2). This is consistent with a delayed but effective onset of innate immunity, as shown previously26,27. At endpoint (43 hpi), pure WT infections infected 16.7 times more cells than pure Δ51 infections. Confirming the interference shown above, in mixed infections the spread of the WT was severely reduced, albeit it still reached 1.26 ± 0.09 more cells than Δ51 at 43 hpi (two-tailed t-test: $P = 0.058$; Fig. 3; Supplementary Fig. 1; Supplementary Video 3).

Altruistic nature of IFN shutdown

Initially, Δ51 spread more efficiently than the WT, reaching 2.43 more cells at 20 hpi. This was not explained by differences between the GFP and mCherry reporters (Supplementary Fig. 2). Furthermore, parallel infections of pure WT versus Δ51 viruses bearing the same GFP reporter confirmed the short-term advantage of Δ51 (Fig. 4a). Thus, before the onset of an effective innate immune response, IFN blockade was costly ($c > 0$). To quantify this cost, we disrupted spatial structure, such that r was minimal and hence $f_W - f_D \approx -c$. For this, we shuffled the cell monolayer twice (8 and 24 hpi) using trypsin, a treatment that should not affect IFN-mediated immunity28. Strikingly, under these conditions Δ51 outcompeted the WT, reaching 2.49 ± 0.18 times more cells at 43 hpi (t-test: $P = 0.001$; Fig. 3). To verify this result, we competed the two variants over three serial transfers in undisturbed versus trypsin-treated MEFs. Whereas the Δ51-GFP variant gradually decreased in frequency throughout transfers in undisturbed cells (Pearson correlation: $\rho = -0.808$, $P = 0.001$), the situation was reversed in trypsin-treated cells ($\rho = 0.753$, $P = 0.005$; Fig. 4b). Finally, we also performed mixed infections in IFN-null, Vero cells. This showed that, in the absence of IFN, the WT was also outcompeted by Δ51 (Supplementary Fig. 3). Overall, this reveals that the WT functions as an altruistic virus ($c > 0$) and that spatial structure ($rb > 0$) is strictly required for selection to favor IFN shutdown. Conversely, Δ51 functions as a social cheater that takes over the population under conditions of low spatial structure even if this reduces population fitness, leading to a “tragedy of the commons”.

Inference of social evolution parameters

In the absence of spatial structure, $r = 0$ and thus $f_W - f_D = -c$. In contrast, if W and D are fully segregated, $r_W = r_D = r = 1$ and thus $f_W - f_D = f_{W/W} - f_{D/D} = b - c$. By comparing these

two scenarios, we determined b and c empirically. For intermediate situations in which the two variants are partially assorted ($0 < r < 1$), we measured f_W and f_D and used the above-estimated b and c to obtain r_D and r_W, since $r_D = (c - f_D)/b$ and $r_W = (f_W + b)/b$. Finally, this allowed us to infer r (Fig. 1). Using fluorescence data (Fig. 3), we calculated log-fitness as $f = \log_{10}A - \log_{10}A_{W/W}$, where A is the area occupied by infected cells and pure WT infections were taken as reference ($f_{W/W} = 0$). We first focused on 43 hpi data, a time point at which the WT was slightly superior to Δ51. Assuming that trypsin removed spatial structure completely, the direct cost of IFN shutdown was $c = 0.394 \pm 0.030$. From pure Δ51 infections, we obtained $f_{D/D} = c - b = -1.221 \pm 0.018$. Hence, $b = 0.393 + 1.221 = 1.615$. From mixed infections, we obtained $f_W = -1.138 \pm 0.060$ and $f_D = -1.236 \pm 0.058$. Thus, the descriptors of spatial structure were $r_D = (c - f_D)/b = 1.009$, $r_W = (f_W + b)/b = 0.295$, and $r = r_D + r_W - 1 = 0.305$. This shows that Δ51 was essentially unaffected by the presence of the WT ($r_D \approx 1$), whereas the WT was strongly inhibited by Δ51 ($r_W < 1$).

To explore parameter time-dependence, we repeated our calculations at 20 hpi, a time point at which Δ51 was still superior to the WT in mixed infections (Fig.3). From trypsin-treated cultures we obtained $c = 0.806 \pm 0.040$. From pure Δ51 infections, $f_{D/D} = -0.538 \pm 0.001$, giving $b = 1.344$. Hence, during late infection (20-43 hpi) the indirect benefits of IFN shutdown (b) increased, whereas direct costs (c) decreased, favoring the WT variant. This suggests a strengthening of paracrine and autocrine responses in the 20-43 hpi range26. From mixed infections we obtained $f_W = -0.942 \pm 0.065$ and $f_D = -0.561 \pm 0.040$ at 20 hpi, thus yielding $r_D = 1.017$, $r_W = 0.299$, and $r = 0.316$. Therefore, r_D, r_W, and r showed little variation in this time range, indicating that the spatial structure of infection and immunity were approximately established by 20 hpi.

Metapopulation structure strongly selects for IFN evasion

As shown above, the WT was inhibited by cytokines secreted from Δ51-infected cells. Yet, viral infections exhibit a marked metapopulation structure in nature in which subpopulations founded by small numbers of transmitted particles remain largely isolated from other subpopulations29–31. This occurs between hosts, but also at the intra-host level as a result of tissue or organ compartmentalization32,33. To demonstrate the role of metapopulation structure in IFN evasion, we mixed Δ51 and WT variants at approximately 1:1 ratio and inoculated MEFs subdivided in 96 wells. We used a limiting dilution of the virus, such that each well typically received 0-2 infectious units. At 48 hpi we determined WT and Δ51 titers. We detected infection in 71/96 wells, of which 20 contained WT only, 35 contained Δ51 only, and 16 contained both variants. In wells with mixed infections, the WT reached higher titers than Δ51 (mean log-titers: 5.34 ± 0.30 and 4.13 ± 0.20, respectively; two-tailed paired t-test: $P < 0.001$; Fig. 5), suggesting intra-well spatial structure, as shown above. Nevertheless, the superiority of the WT was strongly exacerbated in singly infected wells (mean log-titers: 7.00 ± 0.14 and 4.04 ± 0.13 for WT and Δ51, respectively; two-tailed paired t-test: $P < 0.001$). The WT titer indeed increased by 50-fold in pure infections compared to mixed infections (two-tailed t-test: $P < 0.001$), whereas the Δ51 titer remained unchanged (two-tailed t-test: $P = 0.713$). This again confirms that $r_D \approx 1$ and $r_W < 1$. Pooling all wells, 99.4% of the total progeny was produced by the WT, versus 0.6% by Δ51. Hence,

a compartmentalized infection with marked founder effects strongly favored the IFN-blocking virus.

In terms of our model, since the Δ51 virus extracts no benefit from the WT, we can assume a constant log-fitness $f_D = f_{D/D} = c - b$. Assuming no intra-well spatial structure, in mixed groups $f_W - f_D = -c$ (i.e. $r = 0$) and thus $f_W = -b$, whereas in wells containing only WT viruses, $f_W = f_{W/W} = 0$. Intra-well spatial structure can be incorporated into the model by noting that the final log yield per well decays linearly with the initial frequency of the Δ51 virus (Fig. 2b; Supplementary Fig. 4). We found that the overall fitness of W increases with the frequency of pure WT infections, which depends inversely on bottleneck size (Supplementary Fig. 4). Hence, transmission bottlenecks should play an important role in the evolution of viral innate immunity evasion.

In vivo validation of the social nature of IFN shutdown

To explore the relevance of our results in vivo, we inoculated intranasally 15 four-week-old Balb/c mice with approximately 10^8 FFU of VSV WT-mCherry. Nine animals succumbed to the infection by days 7-10 showing typical VSV neurological symptoms (altered behavior, abnormal motility, paralysis). Fluorescence microscopy revealed infection of multiple brain areas, particularly the rostral migratory stream (RMS), thalamus, periventricular areas, and spine bulb (Fig. 6a-c). In parallel, we infected 15 animals with approximately 10^8 FFU of WT-mCherry, plus the same amount of Δ51-GFP. Only two animals exhibited typical VSV symptoms (Fisher exact test: $P = 0.021$). Of these, one showed limb paralysis but no apparent brain infection at endpoint (day 8). In the other animal, infection was restricted to early viral replication sites such as the olfactory bulb (OB) and the anterior RMS (Supplementary Fig. 5), where early IFN signaling is critical for preventing VSV dissemination34. Hence, the Δ51 variant interferes with VSV pathogenicity in vivo.

To assess the relative fitness of Δ51 and WT during early infection, we inoculated nine animals with a 1:1 mix as above and sacrificed three animals at 2, 3, and 4 days post inoculation (dpi) to inspect their brains by fluorescence microscopy. We found no evidence of brain infection at 2 dpi. In one 3 dpi animal and two 4 dpi animals, the virus was restricted to the OB, which showed multiple infected regions. In these three mice, the infection was clearly dominated by Δ51 (Fig. 6d-f). Exhaustive image analysis of these samples showed that GFP encompassed 87.9 ± 7.8 % of the total fluorescent area, indicating that Δ51 was initially superior to the WT (two-tailed t-test: $P = 0.002$; Supplementary Table 1). The brain of the third 4 dpi animal showed a different pattern, since there was no fluorescence in the OB but the WT was found in regions not reached by Δ51 such as the RMS (Supplementary Fig. 6; Supplementary Table 1). Hence, Δ51 spread more efficiently than the WT at early infection sites where it suppressed infection, but the WT occasionally escaped from the inhibitory effects of IFN by reaching more distal regions.

Discussion

We have shown that innate immunity evasion is a social trait in VSV. For this, we have first provided a rationale for the social evolution of IFN shutdown in viruses based on a partition

of viral fitness according to social neighborhood. Then, we have shown experimentally that cytokines produced by cells infected with VSV-Δ51 strongly inhibit the growth of nearby viruses, including the IFN-suppressing WT. Furthermore, we have found that IFN shutdown is costly because Δ51 outcompetes the WT when both viruses share the same neighborhood, that is, in non-assorted populations. Therefore, the evolution of IFN shutdown depends critically on spatial structure, which allows the WT to avoid the interference exerted by the Δ51 variant.

Previous work reported substitutions in the M protein of VSV populations passaged in IFN-deficient cells, including M51 but also S32, Y61, P120, L123, and V22135–39. Molecular characterization of the L123W variant revealed that it impairs the ability of the VSV protein M to block IFN production40, and this mutant was found to interfere with wild-type VSV pathogenicity in vivo41. Furthermore, substitutions P120A, and L123W were shown to confer accelerated growth in IFN-deficient cells42. Therefore, our findings with the Δ51 mutation probably apply to other VSV variants. Considering the fast mutational supply of RNA viruses, the appearance of IFN-stimulating cheater viruses may thus be relatively common. This is suggested by the observation that natural VSV isolates vary amply in their ability to stimulate IFN35,43. Such cheaters could potentially reach high frequencies transitorily, but their ability to invade populations should be curtailed by spatial structure, which is present at many levels including infection foci within tissues, organ compartmentalization, and among individual hosts. In future work, this could be investigated by deep-sequencing natural viral populations at the intra-host level.

VSV WT and Δ51 obey a yield/rate fitness tradeoff because Δ51 initially replicates faster than the WT but reaches a lower final titer. Analogous tradeoffs have been reported in widely different biological systems such as microbial metabolic pathways, in which they also lead to cooperation/cheating dilemmas44. In our system, though, the cheater stimulates the release of an inhibitor that reduces the fitness of all neighbors. This could be relevant to other fast-growth processes producing toxic byproducts such as, for instance, ethanol release during yeast fermentation45. An open question is whether such “pollutants” could promote a coevolution process whereby cooperators evolve resistance to the inhibitor.

Future work may elucidate the mechanistic basis of IFN shutdown costs. At present, we can only speculate that, in VSV, such costs may stem from the multifunctional nature of the M protein. In addition to blocking host gene expression, the M protein is a structural component of the virion. Hence, directing M proteins to block mRNA export might reduce the amount of protein available for virion assembly. Because most RNA virus proteins are highly multifunctional, similar costs could apply to immunity suppressors of other viruses. Alternatively, host gene expression shutdown might reduce the ability of the virus to use cellular factors exported from the nucleus, or trigger apoptosis prematurely.

IFNs have been administered systemically to patients as a non-specific antiviral. Delivery of IFN-stimulating, attenuated viruses might achieve a response more selectively directed towards viral replication sites, potentially increasing efficacy. VSV provides a safe and flexible platform for oncolytic virotherapy46 and has also been used for vaccine design47. Hence, VSV offers in principle a good model for developing “antiviral virotherapy”

strategies based on IFN stimulation. Social evolution principles may prove helpful for achieving this goal, as also suggested for bacteria48.

Methods

Virus

VSV WT-mCherry, WT-GFP, and Δ51-GFP were obtained from an infectious cDNA clone49 kindly provided by Dr. Valery Z. Grdzelishvili (University of North Carolina). Colors were used to track the WT and Δ51 variants. In the event of a reversion of the Δ51 mutation, the association between colors and variants would be lost, but three-base deletions are highly unlikely to revert in the short term. Also, because VSV recombines very infrequently, each variant was stably linked to its corresponding fluorescent reporter.

Cells

MEFs from C57BL/6 mice were isolated as previously described50 and provided by Dr. Carmen Rivas (Universidad de Santiago de Compostela, Spain). BHK-21 (CCL-10) and Vero (CCL-81) cells were purchased from the American Type Culture Collection (ATCC, reference numbers indicated in parentheses). All cells were cultured in Dulbeco's modified Eagle's medium (DMEM) supplemented with 10% fetal bovine serum (FBS) at 37°C in a 5% CO_2 humidified incubator and tested mycoplasma-negative by PCR.

Viral titration

BHK-21 cells were inoculated with various dilutions of the virus, incubated 45 min (37°C, 5% CO_2), and overlaid with DMEM supplemented with 2% FBS containing 0.6% agar. After 20-24 h, cells were fixed with 10% formaldehyde, stained with 2% crystal violet, and used for counting plaques.

Automated real-time fluorescence microscopy

Confluent MEFs in 12-well dishes were inoculated with VSV and kept in an IncuCyte S3 Live-Cell Analysis System (Essen BioScience) at 37°C and 5% CO_2. Images were acquired using phase contrast, green and red channels at 4X magnification. For background correction, raw images were subjected to a top-hat transform using a 100 μm disk. To measure the area occupied by the fluorescence signal, images were segmented by defining a gray-scale intensity threshold such that the fluorescent areas of WT-GFP and WT-mCherry controls were similar (Supplementary Fig. 2). Once defined, the image analysis parameters were kept constant and identical for all experiments. All images share the same saturation values for each channel. For trypsin treatments, the supernatant was collected, cells were washed with PBS, detached with trypsin, spun and washed to remove trypsin, resuspended in the original supernatant, and added back to culture dishes.

Infection and titration in a subdivided MEF population

Confluent MEFs in a 96-well dish were inoculated with a limiting dilution of VSV WT and a NmAb resistant Δ51 mutant mixed at approximately 1:1 ratio. Cultures were incubated for

48 h and supernatants were collected to perform plaque assays in the absence/presence of NmAb, which allowed us to determine the titer of each variant in each well.

Extraction of cytokine-containing medium

Conditioned medium was obtained by infecting a confluent MEF monolayer with VSV Δ51 at an MOI of ca. 3 FFU/cell and collecting the infection medium at 24 hpi. The supernatant was centrifuged at 5000 g for 10 min to remove cellular debris and cleared from virions through a 0.05 μm cellulose filter (MF-Millipore; VMWP02500). The undiluted resulting medium was subjected to the plaque assay to verify the absence of infectious particles.

RT-qPCR

Infected MEFs in 6-well dishes were used for total RNA extraction by the acid guanidinium-thiocyanate-phenol-chloroform method (Invitrogen). Total RNA concentrations were adjusted to 150 ng/μL and subjected to reverse transcription using SuperScript IV (Invitrogen) and specific primers for either mouse Mx2 mRNA (5´tggagtcggattgacatctctg) or β-actin mRNA (5´cagaggcatacagggacagc). RT reactions were carried out at 55°C following manufacturer's instructions. The qPCRs were performed by the SYBR Green method (Agilent) using specific primers for Mx2 (5´acacggtcactgaaattgtacg, 5´tcatcttttcacggttggctt) or β-actin mRNA (5´ctggcaccacaccttctaca, 5´tcatcttttcacggttggctt) under the following cycling conditions: 95°C for 3 min, and 40 cycles of 95°C for 15 s and 60°C for 20 s. RT-qPCR assays were done in triplicate.

ELISA

Supernatants from 24-well dishes were collected, diluted 1:5, and assayed in triplicate with an IFN-β ELISA kit following manufacturer´s instructions (Pierce).

Mouse infections

VSV WT-mCherry and Δ51-GFP were purified in an iodixanol gradient by high-speed centrifugation and used for intranasal inoculation of four-week-old Balb/c (Charles River) females with approximately 0.5-1.0 × 10^8 FFU of pure WT, or a mixture of WT and Δ51 (0.5-1.0 × 10^8 FFU each). The inoculum was administered by aspiration of 10 μL through nostrils. Animals infected with Δ51/WT mixes or pure WT were kept in separate cages and inspected daily for symptoms of infection. Animals showing VSV-induced brain damage symptoms such as severely altered behavior, abnormal motility, or paralysis, as well as other endpoint criteria were euthanized by cervical dislocation or perfused for microscopy analysis. This procedure was approved by the Biosafety Committee and the Animal Welfare Ethics Committee of the Universitat de València and relevant authorities (procedure 2018/VSC/PEA/0029).

Brain fluorescence microscopy

Animals were perfused intracardiacally with NaCl 0.9% followed by PFA 4%. Brains were extracted and incubated overnight in the same fixator, washed in phosphate buffer, and cryopreserved in sucrose 30%. We obtained 25 μm sections in a Leica cryostat, which were stained with DAPI and mounted using Fluorsave reagent (VWR). Sections were analyzed

under a Leica DMi8 fluorescence microscope and image captured with a Leica DFC 3000G camera assisted with proprietary LasX software. To measure the area occupied by GFP- and mCherry-positive cells in OBs, we examined five infected regions per animal, which constituted an exhaustive analysis of the infection. Images were subjected to background correction using a 50 μm (radius) rolling ball, corrected for brightness and contrast, and binarized to measure the fluorescence-positive area. For some images, a two-pixel radius median filter and an erode/dilate process were needed to fit properly the binary mask to the actual fluorescence signal. This analysis was performed with ImageJ/Fiji software.

Supplementary Material

Refer to Web version on PubMed Central for supplementary material.

Acknowledgments

We thank Inma Noguera for technical assistance with the animal experiments, José M. Cuevas, Raquel Garijo and Iván Andreu-Moreno for help with experimental set up, Valery Grdzelishvili for the VSV clones, Carmen Rivas for the MEFs, and Stuart West and Pau Carazo for helpful discussions.

Funding. This work was funded by ERC Consolidator Grant 724519 Vis-a-Vis to R.S. P.D-C. was also funded by a Juan de la Cierva Incorporación postdoctoral contract from Spanish MINECO.

References

1. Nowak MA. Five rules for the evolution of cooperation. Science. 2006; 314:1560–1563. [PubMed: 17158317]
2. Fletcher JA, Doebeli M. A simple and general explanation for the evolution of altruism. Proc Biol Sci. 2009; 276:13–19. [PubMed: 18765343]
3. Gardner A, West SA, Wild G. The genetical theory of kin selection. J Evol Biol. 2011; 24:1020–1043. [PubMed: 21371156]
4. Díaz-Munoz SL, Sanjuán R, West S. Sociovirology: conflict, cooperation, and communication among viruses. Cell Host Microbe. 2017; 22:437–441. [PubMed: 29024640]
5. Turner PE, Chao L. Prisoner's dilemma in an RNA virus. Nature. 1999; 398:441–443. [PubMed: 10201376]
6. Skums P, Bunimovich L, Khudyakov Y. Antigenic cooperation among intrahost HCV variants organized into a complex network of cross-immunoreactivity. Proc Natl Acad Sci USA. 2015; 112:6653–6658. [PubMed: 25941392]
7. Erez Z, et al. Communication between viruses guides lysis-lysogeny decisions. Nature. 2017; 541:488–493. [PubMed: 28099413]
8. Borges AL, et al. Bacteriophage cooperation suppresses CRISPR-Cas3 and Cas9 immunity. Cell. 2018; 174:917–925 e910. [PubMed: 30033364]
9. Xue KS, H KA, Ollodart AR, Dingens AS, Bloom JD. Cooperation between distinct viral variants promotes growth of H3N2 influenza in cell culture. Elife. 2016; 5:e13974. [PubMed: 26978794]
10. Leggett HC, Brown SP, Reece SE. War and peace: social interactions in infections. Philos Trans R Soc Lond B Biol Sci. 2014; 369
11. Xavier JB. Sociomicrobiology and pathogenic bacteria. Microbiol Spectr. 2016; 4
12. Ivashkiv LB, Donlin LT. Regulation of type I interferon responses. Nat Rev Immunol. 2014; 14:36–49. [PubMed: 24362405]
13. Fensterl V, Chattopadhyay S, Sen GC. No love lost between viruses and interferons. Annu Rev Virol. 2015; 2:549–572. [PubMed: 26958928]
14. García-Sastre A. Ten strategies of interferon evasion by viruses. Cell Host Microbe. 2017; 22:176–184. [PubMed: 28799903]

Europe PMC Funders Author Manuscripts

15. Coccia EM, Battistini A. Early IFN type I response: learning from microbial evasion strategies. Semin Immunol. 2015; 27:85–101. [PubMed: 25869307]
16. Lion S, Jansen VA, Day T. Evolution in structured populations: beyond the kin versus group debate. Trends Ecol Evol. 2011; 26:193–201. [PubMed: 21353325]
17. Birch J. Kin selection, group selection, and the varieties of population structure. Brit J Phil Sci. 2018; doi: 10.1093/bjps/axx028
18. Lehtonen J. Multilevel selection in kin selection language. Trends Ecol Evol. 2016; 31:752–762. [PubMed: 27590987]
19. Marshall JA. Group selection and kin selection: formally equivalent approaches. Trends Ecol Evol. 2011; 26:325–332. [PubMed: 21620513]
20. West SA, Griffin AS, Gardner A, Diggle SP. Social evolution theory for microorganisms. Nat Rev Microbiol. 2006; 4:597–607. [PubMed: 16845430]
21. O'Brien S, Luján AM, Paterson S, Cant MA, Buckling A. Adaptation to public goods cheats in *Pseudomonas aeruginosa*. Proc Biol Sci. 2017; 284
22. Jin Z, et al. Conditional privatization of a public siderophore *enables Pseudomonas aeruginosa* to resist cheater invasion. Nat Commun. 2018; 9
23. Rajani KR, et al. Complexes of vesicular stomatitis virus matrix protein with host Rae1 and Nup98 involved in inhibition of host transcription. PLoS Pathog. 2012; 8:e1002929. [PubMed: 23028327]
24. Quan B, Seo HS, Blobel G, Ren Y. Vesiculoviral matrix (M) protein occupies nucleic acid binding site at nucleoporin pair (Rae1 * Nup98). Proc Natl Acad Sci USA. 2014; 111:9127–9132. [PubMed: 24927547]
25. Stojdl DF, et al. VSV strains with defects in their ability to shutdown innate immunity are potent systemic anti-cancer agents. Cancer Cell. 2003; 4:263–275. [PubMed: 14585354]
26. Voigt EA, Swick A, Yin J. Rapid induction and persistence of paracrine-induced cellular antiviral states arrest viral infection spread in A549 cells. Virology. 2016; 496:59–66. [PubMed: 27254596]
27. Howat TJ, Barreca C, O'Hare P, Gog JR, Grenfell BT. Modelling dynamics of the type I interferon response to in vitro viral infection. J R Soc Interface. 2006; 3:699–709. [PubMed: 16971338]
28. Samuel CE, K GS. Mechanism of interferon action. Kinetics of decay of the antiviral state and protein phosphorylation in mouse fibroblasts treated with natural and cloned interferons. J Biol Chem. 1982; 257:6.
29. Zwart MP, Elena SF. Matters of size: genetic bottlenecks in virus infection and their potential impact on evolution. Annu Rev Virol. 2015; 2:161–179. [PubMed: 26958911]
30. Gutiérrez S, Michalakis Y, Blanc S. Virus population bottlenecks during within-host progression and host-to-host transmission. Curr Opin Virol. 2012; 2:546–555. [PubMed: 22921636]
31. McCrone JT, Lauring AS. Genetic bottlenecks in intraspecies virus transmission. Curr Opin Virol. 2018; 28:20–25. [PubMed: 29107838]
32. Richard M, Herfst S, Tao H, Jacobs NT, Lowen AC. Influenza A virus reassortment is limited by anatomical compartmentalization following co-infection via distinct routes. J Virol. 2017; doi: 10.1128/JVI.02063-17
33. Salemi M, Rife B. Phylogenetics and phyloanatomy of HIV/SIV intra-host compartments and reservoirs: the key role of the central nervous system. Curr HIV Res. 2016; 14:110–120. [PubMed: 26511341]
34. Detje CN, et al. Local type I IFN receptor signaling protects against virus spread within the central nervous system. J Immunol. 2009; 182:2297–2304. [PubMed: 19201884]
35. Francoeur AM, Poliquin L, Stanners CP. The isolation of interferon-inducing mutants of vesicular stomatitis virus with altered viral P function for the inhibition of total protein synthesis. Virology. 1987; 160:236–245. [PubMed: 2820131]
36. Novella IS, Hershey CL, Escarmís C, Domingo E, Holland JJ. Lack of evolutionary stasis during alternating replication of an arbovirus in insect and mammalian cells. J Mol Biol. 1999; 287:459–465. [PubMed: 10092452]
37. Cuevas JM, Elena SF, Moya A. Molecular basis of adaptive convergence in experimental populations of RNA viruses. Genetics. 2002; 162:533–542. [PubMed: 12399369]

38. Remold SK, Rambaut A, Turner PE. Evolutionary genomics of host adaptation in vesicular stomatitis virus. Mol Biol Evol. 2008; 25:1138–1147. [PubMed: 18353798]
39. Morita K, Vanderoef R, Lenard J. Phenotypic revertants of temperature-sensitive M protein mutants of vesicular stomatitis virus: sequence analysis and functional characterization. J Virol. 1987; 61:256–263. [PubMed: 3027358]
40. Brun J, et al. Identification of genetically modified Maraba virus as an oncolytic rhabdovirus. Mol Ther. 2010; 18:1440–1449. [PubMed: 20551913]
41. Furió V, et al. Relationship between within-host fitness and virulence in the vesicular stomatitis virus: vorrelation with partial decoupling. J Virol. 2012; 86:12228–12236. [PubMed: 22951843]
42. Sanjuán R, Moya A, Elena SF. The distribution of fitness effects caused by single-nucleotide substitutions in an RNA virus. Proc Natl Acad Sci USA. 2004; 101:8396–8401. [PubMed: 15159545]
43. Marcus PI, Rodríguez LL, Sekellick MJ. Interferon induction as a quasispecies marker of vesicular stomatitis virus populations. J Virol. 1998; 72:542–549. [PubMed: 9420257]
44. Pfeiffer T, Schuster S, Bonhoeffer S. Cooperation and competition in the evolution of ATP-producing pathways. Science. 2001; 292:504–507. [PubMed: 11283355]
45. Stanley D, Bandara A, Fraser S, Chambers PJ, Stanley GA. The ethanol stress response and ethanol tolerance of *Saccharomyces cerevisiae*. J Appl Microbiol. 2010; 109:13–24. [PubMed: 20070446]
46. Hastie E, Grdzelishvili VZ. Vesicular stomatitis virus as a flexible platform for oncolytic virotherapy against cancer. J Gen Virol. 2012; 93:2529–2545. [PubMed: 23052398]
47. Clarke DK, et al. Live virus vaccines based on a vesicular stomatitis virus (VSV) backbone: standardized template with key considerations for a risk/benefit assessment. Vaccine. 2016; 34:6597–6609. [PubMed: 27395563]
48. Brown SP, West SA, Diggle SP, Griffin AS. Social evolution in micro-organisms and a Trojan horse approach to medical intervention strategies. Philos Trans R Soc Lond B Biol Sci. 2009; 364:3157–3168. [PubMed: 19805424]
49. Lawson ND, Stillman EA, Whitt MA, Rose JK. Recombinant vesicular stomatitis viruses from DNA. Proc Natl Acad Sci USA. 1995; 92:4477–4481. [PubMed: 7753828]
50. Palmero I, Serrano M. Induction of senescence by oncogenic Ras. Methods Enzymol. 2001; 333:247–256. [PubMed: 11400340]

Europe PMC Funders Author Manuscripts

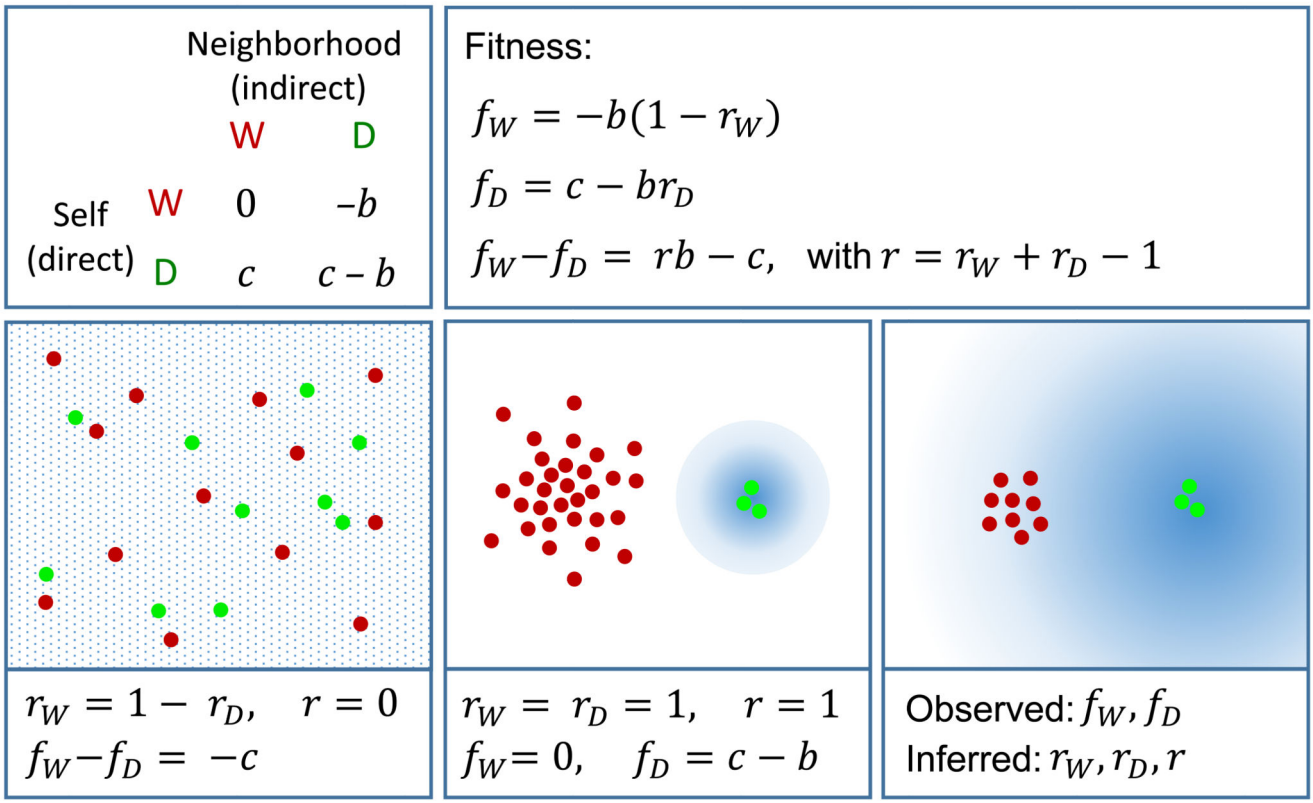

Fig. 1. Social evolution model for innate immunity evasion.

Top left: partition of individual fitness according to social neighborhood. One virus blocks IFN (W) and another that does not (D). The W virus in a W neighborhood is used as reference and has log fitness (*f*) equal to zero. IFN-mediated paracrine signaling has an indirect fitness effect *b* that applies to W and D. The direct effect of blocking IFN on the actor, independent of neighborhood effects, is denoted *c*, and can a priori be positive or negative. Because fitness is defined logarithmically, independent effects are additive and hence the fitness of D in a D neighborhood is $c - b$. Top right: fitness of each variant, which depends on spatial structure through r_W and r_D. Bottom: three possible scenarios (W-infected cells in red, D-infected cells in green, region of immunized cells in blue). Bottom left: no spatial structure, both viruses share the same neighborhood. Bottom middle: maximal spatial structure. Analysis of these two cases allows obtaining *b* and *c*. Bottom right: intermediate situation. If f_W and f_D are measured and *b* and *c* are known, r_W, r_D, and *r* can be inferred.

Europe PMC Funders Author Manuscripts

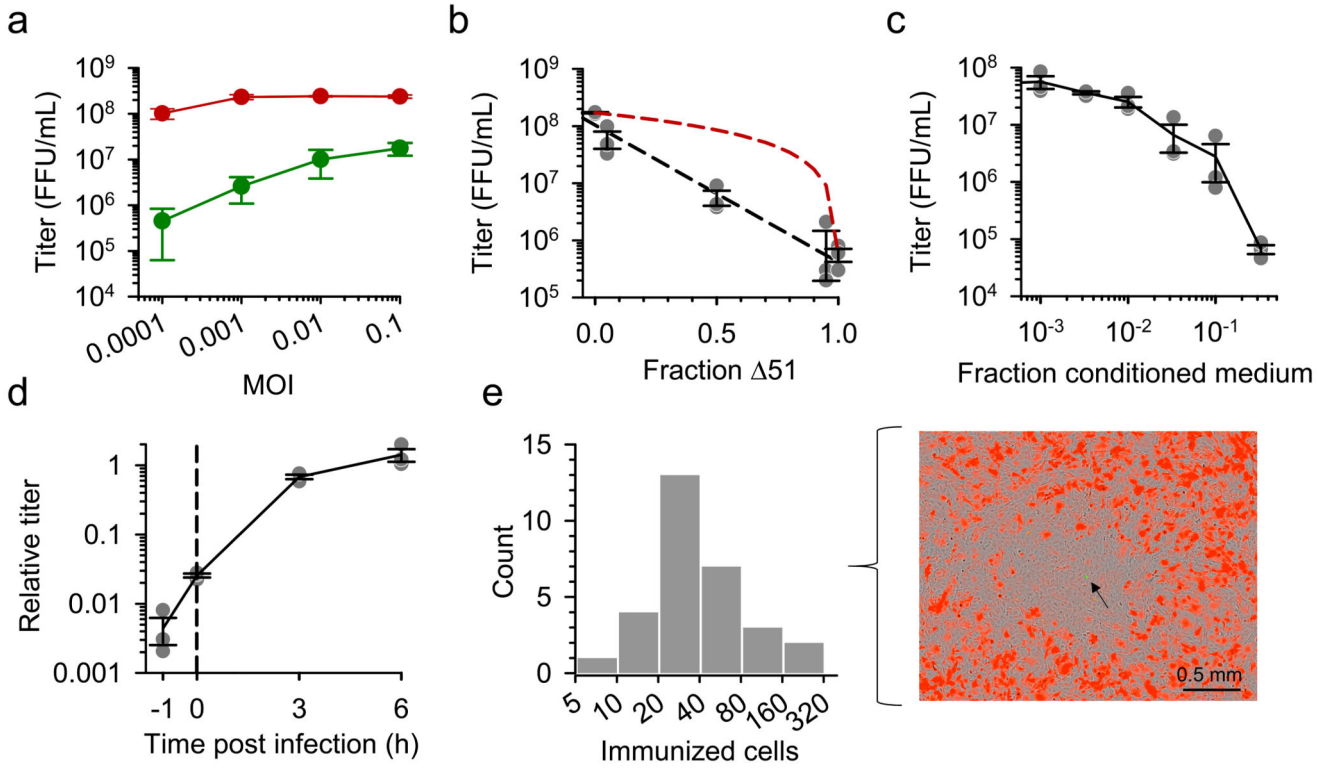

Fig. 2. Interaction between VSV WT and Δ51 variants.

a. Maximal titers of Δ51 (green) and WT (red) in mono-infected cultures at 45 hpi. **b.** Total titers at 45 hpi in cultures infected with Δ51 and WT at different input ratios (MOI = 0.001 FFU/cell). The black dashed line shows the least-squares linear regression. The red dashed line shows the expected total titer assuming no interaction between the two variants. This was obtained based on the titers reached by pure WT and Δ51 infections as follows: $T(p) = pT_{\Delta 51} + (1 - p)\ T_{WT}$, where T is titer, p is the fraction of Δ51 at inoculation, and $T_{\Delta 51}$ and T_{WT} are the titers reached by pure Δ51 and WT infections, respectively. **c**. WT titer at 45 hpi in MEFs primed for 1 h with a conditioned medium obtained from a previous Δ51 infection (MOI = 0.001 FFU/cell). **d**. Time-dependence of anti-VSV IFN effects. MEFs were treated with a 1/5 dilution of conditioned medium at the indicated times. All treatments reduced titer significantly (one sample t-tests against 1.0: $P = 3.5 \times 10^{-6}$, $P = 2.9 \times 10^{-6}$, and $P = 0.024$ for t = – 1 hpi, 0 hpi, and 3 hpi, respectively) except the 6 hpi treatment ($P = 0.290$). In **a-d** error bars indicate the SEM of n = 3 independent measures, and in **b-d** the three individual data points are also shown. **e.** Range of action of innate immune signaling from single Δ51-infected cells. In the picture, a single cell infected with Δ51 (GFP-positive, apoptotic, shown with arrow) generates a region of cells resistant to the WT virus (lack of red fluorescence). The approximate size of the immunized region was determined by visual inspection. Histogram: distribution of the number of immunized cells obtained after analyzing 30 images (mean: 54.0 ± 9.6 cells).

Europe PMC Funders Author Manuscripts

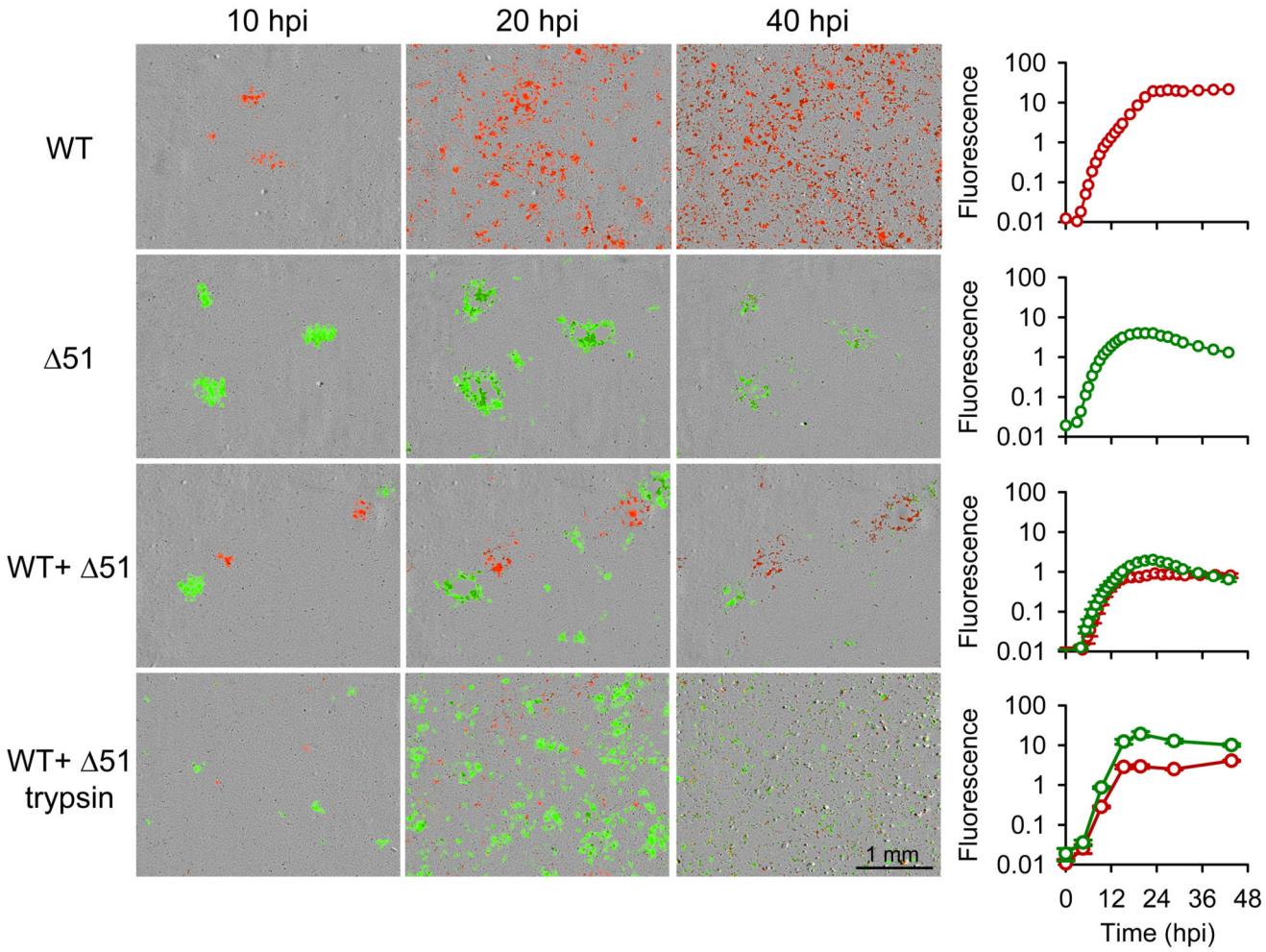

Fig. 3. Real-time fluorescence microscopy of VSV WT and Δ51 in MEFs.

Pure WT-mCherry, pure Δ51-GFP, and mixed WT-mCherry/Δ51-GFP infections were carried out in the same w12 multi-well dish, which also included mixed WT-mCherry/WT-GFP controls (Supplementary Fig. 2). Left: representative images of three time points. Right: average area occupied by GFP and mCherry signals (n = 2 replicate wells for pure WT and Δ51 infections, n = 4 replicates for mixed infections). Notice that these graphs were obtained by image analysis of entire culture wells, not just the representative images shown on the left panels. SEM values correspond to the technical error among wells of the same experimental block. Two additional experimental blocks were performed with similar results. For the trypsin treatment (performed at 8 and 24 hpi), fewer data points were analyzed because cell detachment prevented imaging at each time point. This treatment was performed in a separate w12 well, which included its own controls (Supplementary Fig. 2). The progression of the infection is shown in Supplementary Videos 1-3, and whole-well images are shown in Supplementary Fig. 1.

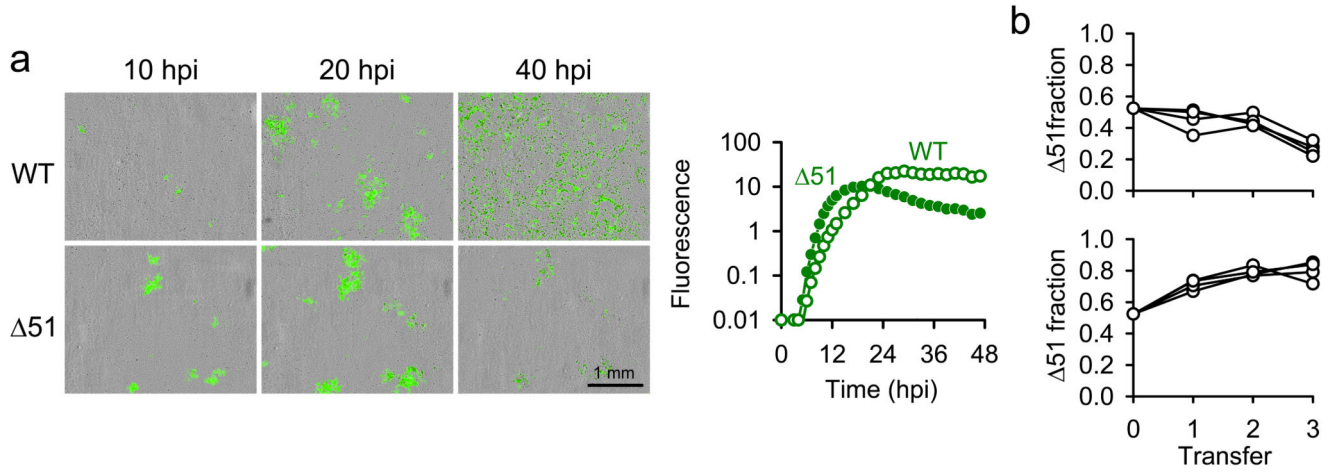

Fig. 4. Fitness cost of IFN shutdown.

a. Spread of pure VSV WT-GFP and pure VSV Δ51-GFP infections. Left: representative images of three time points. Right: average area occupied by the GFP signal (n = 2 replicate wells). Notice that these graphs were obtained by image analysis of entire culture wells, not just the representative images shown on the left panels. Infections were carried out in the same multi-well dish (experimental block), and image acquisition/analysis was performed identically for all wells. Similar results were obtained in another experimental block. **b.** Competition assays between VSV WT-mCherry and Δ51-GFP. Three 48 hpi transfers were performed in undisturbed cells (top) and in cells subjected to trypsin treatment at 8 and 24 hpi (bottom). The Δ51 fraction (GFP/total fluorescent area) after each transfer is shown. Each of the n = 4 lines represents one replicate of the competition assay.

Europe PMC Funders Author Manuscripts

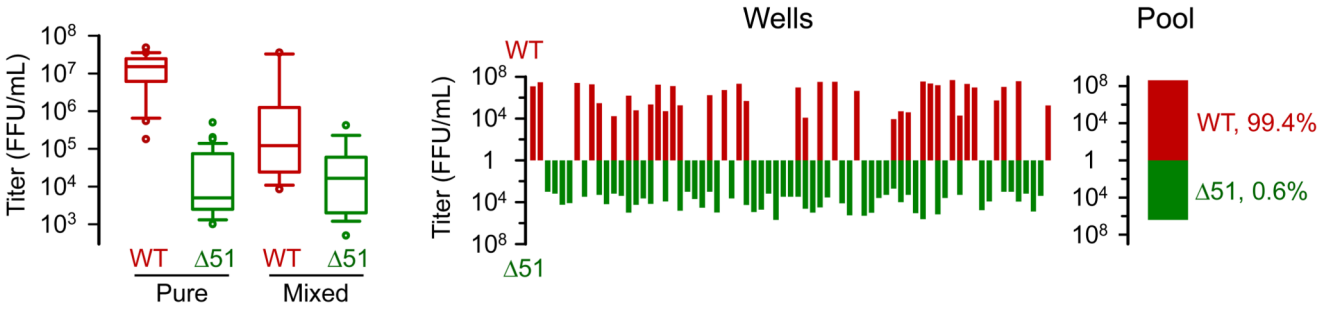

Fig. 5. Metapopulation structure selects for IFN shutdown.

MEFs in a 96-well format were inoculated with a limiting dilution of an approximately 1:1 mix of the WT and a NmAb-resistant Δ51 virus. Titers produced by each variant in each well were determined by the plaque assay. Left: Box plots of the WT and Δ51 titers in wells showing only one variant (pure; n = 20 for WT and n = 35 for Δ51) or a mixture of the two variants (mixed; n = 16). The lower and upper limits of the box indicate 25th and 75th percentiles, and the middle line shows the median. Whiskers show the 10th and 90th percentiles, and outlying points are plotted individually. Middle: titers produced in each individual well. Right: overall WT and Δ51 yield in the metapopulation (sum of all wells).

Europe PMC Funders Author Manuscripts

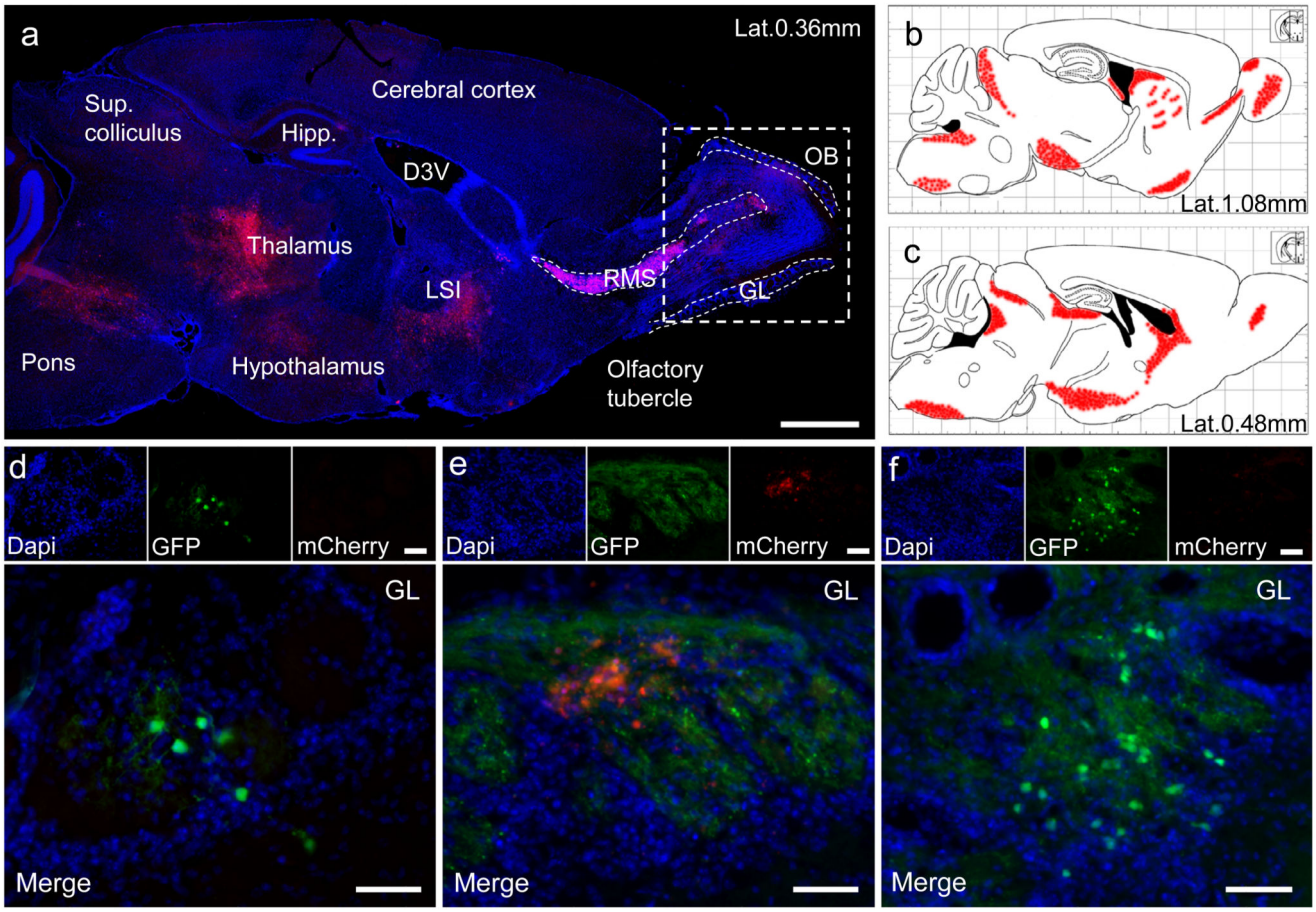

Fig. 6. Fluorescence microscopy of VSV-infected mouse brains.

a. Brain full sagittal section (except cerebellum) of a mouse succumbing to an infection by VSV WT-mCherry (nuclei stained with DAPI). Scale bar: 1 mm. **b, c.** Atlases showing a schematic representation of the infection pattern observed in two additional, parallel sections. Given that animals were inoculated intranasally, the observed pattern is consistent with primary infection of the OB glomerular layer (GL) originating from olfactory axons and spreading along the RMS. Isolated infected areas were also found in the olfactory tubercle. The infection may have progressed from the RMS towards lateral ventricles, producing infected areas adjacent to ventricular walls (lateral septal nucleus, striatum adjacent to the anterior region of the lateral ventricle, and hippocampus adjacent to the posterior ventricle). Hence, the ventricular system probably acted as a route for disseminating the infection towards the thalamus and hypothalamus. The thalamus appears as another major infection site, from which the virus may have reached the spinal cord, producing paralysis. Examination of the brains from two additional animals inoculated with WT-mCherry showed similar infection patterns. The OB of a pure WT infection and OB/RMS regions of a mixed infection are shown in Supplementary Fig. 5. d-f. Individual infected regions in the OB glomerular layer of n = 3 mice infected with a 1:1 mix of WT-mCherry and Δ51-GFP, one at 3 dpi (**d**) and two at 4 dpi (**e, f**). Scale bars: 50 μm. In these

Europe PMC Funders Author Manuscripts

three animals, no signs of infection were found in the rest of the brain. Quantitation of the area occupied by Δ51-GFP and WT-mCherry is shown on Supplementary Table 1.

Europe PMC Funders Author Manuscripts